

Article

Thermodynamic, Exergy and Environmental Impact Assessment of S-CO₂ Brayton Cycle Coupled with ORC as Bottoming Cycle

Edwin Espinel Blanco ¹, Guillermo Valencia Ochoa ^{2,*}  and Jorge Duarte Forero ² 

¹ Facultad de Ingeniería, Universidad Francisco de Paula Santander, Vía Acolsure. Sede el Algodonal Ocaña, Ocaña-Norte de Santander 546552, Colombia; eeespinelb@ufps.edu.co

² Programa de Ingeniería Mecánica, Universidad del Atlántico, Carrera 30 Número 8–49, Puerto Colombia, Barranquilla 080007, Colombia; jorgeduarte@mail.uniatlantico.edu.co

* Correspondence: guillermoevalencia@mail.uniatlantico.edu.co; Tel.: +575-324-94-31

Received: 22 March 2020; Accepted: 29 April 2020; Published: 4 May 2020



Abstract: In this article, a thermodynamic, exergy, and environmental impact assessment was carried out on a Brayton S-CO₂ cycle coupled with an organic Rankine cycle (ORC) as a bottoming cycle to evaluate performance parameters and potential environmental impacts of the combined system. The performance variables studied were the net power, thermal and exergetic efficiency, and the brake-specific fuel consumption (BSFC) as a function of the variation in turbine inlet temperature (TIT) and high pressure (P_{HIGH}), which are relevant operation parameters from the Brayton S-CO₂ cycle. The results showed that the main turbine (T1) and secondary turbine (T2) of the Brayton S-CO₂ cycle presented higher exergetic efficiencies (97%), and a better thermal and exergetic behavior compared to the other components of the System. Concerning exergy destruction, it was found that the heat exchangers of the system presented the highest exergy destruction as a consequence of the large mean temperature difference between the carbon dioxide, thermal oil, and organic fluid, and thus this equipment presents the greatest heat transfer irreversibilities of the system. Also, through the Life Cycle Analysis, the potential environmental impact of the system was evaluated to propose a thermal design according to the sustainable development goals. Therefore, it was obtained that T1 was the component with a more significant environmental impact, with a maximum value of 4416 Pts when copper is selected as the equipment material.

Keywords: Brayton; environmental impact; exergy; life cycle analysis; ORC; performance parameters

1. Introduction

With the reinforcement of environmental legislation, emission mitigation continues to be an essential problem at the industrial level, and heat recovery in manufacturing procedures is becoming standard practice because of progressively stringent policies on energy efficiency [1]. Therefore, waste heat recovery systems play an essential role in saving energy by considering existing energy generation technologies that are geared towards reducing fuel consumption, greenhouse emissions, and electricity production cost [1]. For this reason, the volume of power and temperature, as well as the form and the prices of technologies for the recovering of waste resources, are the key factors determining the feasibility of energy consumed. Accordingly, to reach a maximum recovery capacity, it is of particular significance that the temperature and the residual heat correlate with the energy recovery periods for the remaining electricity [1].

For alternative energy generation, the concept of the simple regeneration process has been suggested, considering CO₂ as a working solvent due to its properties [2], including low critical

strain, high thermal tolerance at interest temperature, inertia, well known thermal properties, as well as being nontoxic and economical. Angelino et al. [3] published research related to various cycle designs. They demonstrated that the recompression cycle is better at high temperatures, and it is particularly interesting in high-temperature gas-cooled reactors. Subsequently, Dostal et al. [4] in his thesis evaluated the Brayton S-CO₂ cycle for advanced nuclear power generation reactors.

Nowadays, many organic Rankine cycle (ORC) applications have been used as a waste heat recovery system to convert waste heat into mechanical energy. However, the ORC has efficiency limitations when working with waste heat at high temperatures because of the physical and thermal properties usually presented by organic fluids. Abrosimov et al. [5] investigated the combination of a Brayton cycle and an ORC cycle by designing both ORC and combined cycle models using Aspen Hysys® version 9 (Aspen Technology, Inc., Bedford, MA, USA). Thermodynamic and economic optimizations of the models were made to conduct a comparative analysis between the solutions. The results have demonstrated the 10% advantage of the combined scheme over the ORC cycle in terms of generated power and system efficiency. Optimization based on the leveled energy cost for variable capacity factors has revealed an advantage of more than 6% of the solution investigated.

Zhangpeng Guo et al. [6] conducted a sensitivity analysis comparing the recompression cycle, the double-expansion recompression cycle, and the modified recompression cycle applied to fourth-generation nuclear reactors, which have high operating temperatures and pressures that would increase plant efficiency and hydrogen production. Vasquez Padilla et al. [7] conducted a detailed energy and exergy analysis of four Brayton S-CO₂ cycle configurations (single Brayton cycle, recompression Brayton cycle, partial cooling recompression, and main compression with intercooling) with and without reheating to investigate the effect of replacing the reheater and heater by a solar receiver. In the same year, Ricardo Vásquez et al. [8] also performed the energy and exergy analysis of a supercritical Brayton cycle with recompression CO₂, but a bottoming cycle was not proposed.

In recent decades, the Brayton S-CO₂ cycle has attracted the attention of many academics and industries because of its significant advantages [3,9], such as a better thermal efficiency [10]. Brayton S-CO₂ is less caustic relative to steam with the same operating speed, the turbomachine used is lightweight, almost ten times smaller than the steam turbine, and dry cooled easily in comparison with the steam engine [11]. Therefore, based on each of these benefits, the Brayton S-CO₂ cycle has been tested for various uses as an energy conversion device, including nuclear, geothermal, solar, and thermal power plants. So, the device presents higher thermal performance and a smaller process size than the traditional Rankine steam device based on these advantages, and therefore the Brayton S-CO₂ cycle is considered an efficient alternative to the steam process at Rankine [12].

The thermal performance of the heat exchanger plays an important role in the cycle efficiency, as shown in these previously described studies [13]. Thus, when a significant amount of heat is extracted in the recuperator to improve thermal performance, the high energy output is expected and thus the capital cost decreases by utilizing traditional shell and tube heat exchangers (STHE); nonetheless, some high-compact heat exchangers (up to ten times relative to STHE) and printed circuit heat exchangers (PCHE) have been sold and can be added directly to waste heat recovery from gas [14]. However, this type of heat exchanger can be multi-objective optimized, attending to exergy and energy objective function [15]. Yuan Jiang et al. [16] published a paper detailing the core architecture and optimization methodology built into the Aspen Custom Modeler for microtube shell and tube exchangers. They also sized a PCHE and then compared it among the various heat exchangers used for S-CO₂ and indicated that the PCHE is a promising candidate due to its concentration, quick dynamic response, and mature construction state. Optimum configuration findings suggest that there is less metal mass in a system of two hot plates per cold plate and high angle channels; therefore, a safer option for broad-scale applications [17].

The PCHE is a type of micro-channel heat exchanger residing in various carve sheets composed of many micro-waved channels in each layer [18]. Thus, Devesh Ranjan et al. [19] in 2019 developed experimental research in which the characteristics of heat flow and pressure drop decrease for the

PCHE with a different configuration, which is a promising result increasing the thermal performance of the S-CO₂ integrated with ORC.

All this research involves a substantial economic investment; however, there is an effective way with a high degree of reliability to perform these tests without the need for tuning, and that is through dynamic modeling. In engineering, dynamic modeling and simulation are increasingly relevant, as there is a growing need to study the chaotic function of complex structures made up of components from different domains. The models may be used to conduct danger and operability tests. Automated emergency response protocols were validated in [20], as in the case of Xiaoyan Ji et al. [18] also, who performed the heat exchanger design for the suspensions in biogas plants, which was analyzed numerically based on the rheological properties and further coupled with full thermal cycles to demonstrate waste heat recovery and high heating capacity for heat exchangers design. Dynamic models may help design heat-sharing facilities [21]. For example, Oh Jong-Taek et al. [22] demonstrated employing computational fluid dynamics to study the heat transfer and flow characteristics, as well as the effect of mass flow on temperature and pressure distribution in PCHE.

On the other hand, the Brayton S-CO₂ cycles help to predict the advantages of compact equipment within the moderate temperature range (450–750 °C), as well as finding the disadvantages of materials due to high temperatures and pressure, studied in various applications [23,24]. Craig S. Turchi et al. [25] using simulations of the Brayton S-CO₂ cycle, observed favorable characteristics such as the capacity to adapt dry cooling and produce the desired efficiency in the area of solar energy concentration. Yann Le Moullec [26] proposed a closed Brayton S-CO₂ loop based on combining carbon capture and storage facilities to mitigate CO₂ pollution as electricity production from coal-fired power plants is a significant source of ambient CO₂ pollution, as Olumide Olumayegun et al. [27] where the thermodynamic performance of Brayton S-CO₂ cycles coupled to a coal furnace and integrated with 90% post-combustion CO₂ capture was evaluated, investigating three background s-CO₂ cycle designs, including a new recompression cycle with a single recuperator, showing as a result, that the configuration with a recompression cycle and a single recuperator has the highest net plant efficiency. Without CO₂ capture, the effectiveness of the coal-fired plants was higher than that of steam. Youcan Liang et al. [28], shows the application of the method on a dual-fuel engine, which reveals that the maximum net power of the system is up to 40.88 kW, improving by 6.78%, leading to greater energy efficiency and reduced fuel consumption of the engine. Complementarily, Shih-Ping Kao et al. [29] released the results of a complex simulation code based on actual gas and integral momentum models, which was developed at the Massachusetts Institute of Technology to test control strategies for a small light-water reactor fitted with a compact Brayton S-CO₂ cycle.

Based on the significant energy loss presented in the industrial generation engine, some waste heat recovery systems based on the Brayton S-CO₂ cycle have been studied. Therefore, in 2018 Antti Uusitalo et al. [30] examined the use of supercritical Brayton cycles to recover power from the exhaust gases of large-scale engines. The objective of this study was to examine electricity generation through varying operating conditions and organic fluids and thus define the key design parameters influencing the cycle's energy output. In 2018 Piero Danieli et al. [31] measured the economic and thermodynamic efficiency of four separate waste heat recovery systems implemented through simulation to two hollow glass furnaces producing around 4 MWt of heat loss at 450 °C. Also, Subhash Lahane et al. [32] planned a heat exchanger design to collect the excess heat from the exhaust gases of a diesel engine to preheat the air entering the combustion chamber; this should be situated between the engine's inlet and outlet ducts.

However, it is also possible to determine optimal operating conditions of the combined Brayton-ORC system through advanced exergetic analysis, as in the case of Valencia et al. [33], where the fluid is selected to perform an advanced exergetic analysis in a combined thermal system using the ORC as bottoming cycle of an internal combustion engine, finding improvements of up to 80% in the components of the process. The thermo-economic analyses had been used to optimize the components of a trigeneration system, constituted by a gas microturbine and a heat recovery steam

generation sub-system [34]. In addition, the ORC as a bottoming cycle of an internal combustion engine was proposed, identifying the heat transfer equipment with the highest exergy destruction costs, representing 81.25% of the total system cost, and acetone as the working fluid with the best impact on reducing these costs [35]. Another approach to determining optimal operating conditions is to conduct mathematical modeling of the physical phenomena. So, a phenomenologically based semi-physical model for a 2 MW internal combustion engine was obtained as a function of average thermodynamic value, validated by real operating data, to predict the thermodynamic performance parameters of the bottoming cycle as waste heat recovery systems [36].

The above studies propose heat recovery with bottoming cycles, using the different thermal power configurations, modeling the cycle components or making simulations of the same, including economic optimization in one of them; leaving with a wide uncertainty gap regarding the performance of this cycle integrated to ORC as bottoming cycle, which, despite not handling high temperatures, is a challenge in terms of designing a highly efficient heat exchanger so that high thermal performance of the combined power cycle can be obtained.

Therefore, the main contribution of this research is to present a thermodynamic, exergy, and environmental parametric study of a proposed combined S-CO₂ and ORC as a bottoming cycle considering the toluene, cyclohexane, and acetone as the organic working fluids. The methodology of the life cycle analysis is applied to investigate the environmental impact of the components of the system during its lifetime, which allows for the evaluation of environmental impacts, and the determination of energetic and exergetic improvement potentials for the environmental sustainability of the system.

2. Methodology

2.1. Description and Properties of the System

The system shown in Figure 1 is an ORC configuration combined with a Brayton S-CO₂ cycle. The Brayton cycle consists of the following components: the primary turbine (T1), a secondary turbine (T2), an axial compressor (C1), a reheater (RH), and a recuperator (HTR). The ORC cycle includes a shell and tube heat exchanger (ITC1), an evaporator (ITC2), a condenser (ITC3), a thermal oil circuit pump (P1), an organic fluid pump (P2), and a turbine (T3).

In the process, the carbon dioxide enters the primary turbine (T1) of the Brayton cycle at point 1, at a high temperature and pressure, then enters to the reheater (RH) at point 2 and is expanded to lower pressure in the secondary turbine (T2). Next, by means of the recuperator (HTR), the carbon dioxide (point 7) that leaves the compressor (C1) is reheated, which is conducted to the heater (RH) to obtain the thermodynamic state reported as (point 8). Meanwhile, the fluid in point 5 is cooled by yielding heat to the thermal oil, and then it is compressed by the compressor (C1) at point 6.

In the ORC, the thermal oil (Therminol 75) receives heat in the heat exchanger (ITC1) to be transferred to the evaporator (ITC2). During this process, there are three stages: preheating, evaporation, and overheating, with the purpose of heat the organic fluid (Cyclohexane, Toluene, Acetone), while the thermal oil flow through the cycle with the energy supply by the pump (P1). Then, the organic fluid enters the turbine (T3) at a high temperature and pressure through the 1ORC current and expands to decrease its pressure and temperature to enter the condenser (ITC3), where the water cools it at room temperature (point 1A), and then goes to the reservoir (2A). Subsequently, when the organic working fluid leaves the condenser (ITC3) at point 3ORC, it enters the pump (P2) as a saturated liquid and then completes the cycle entering the evaporator (ITC2).

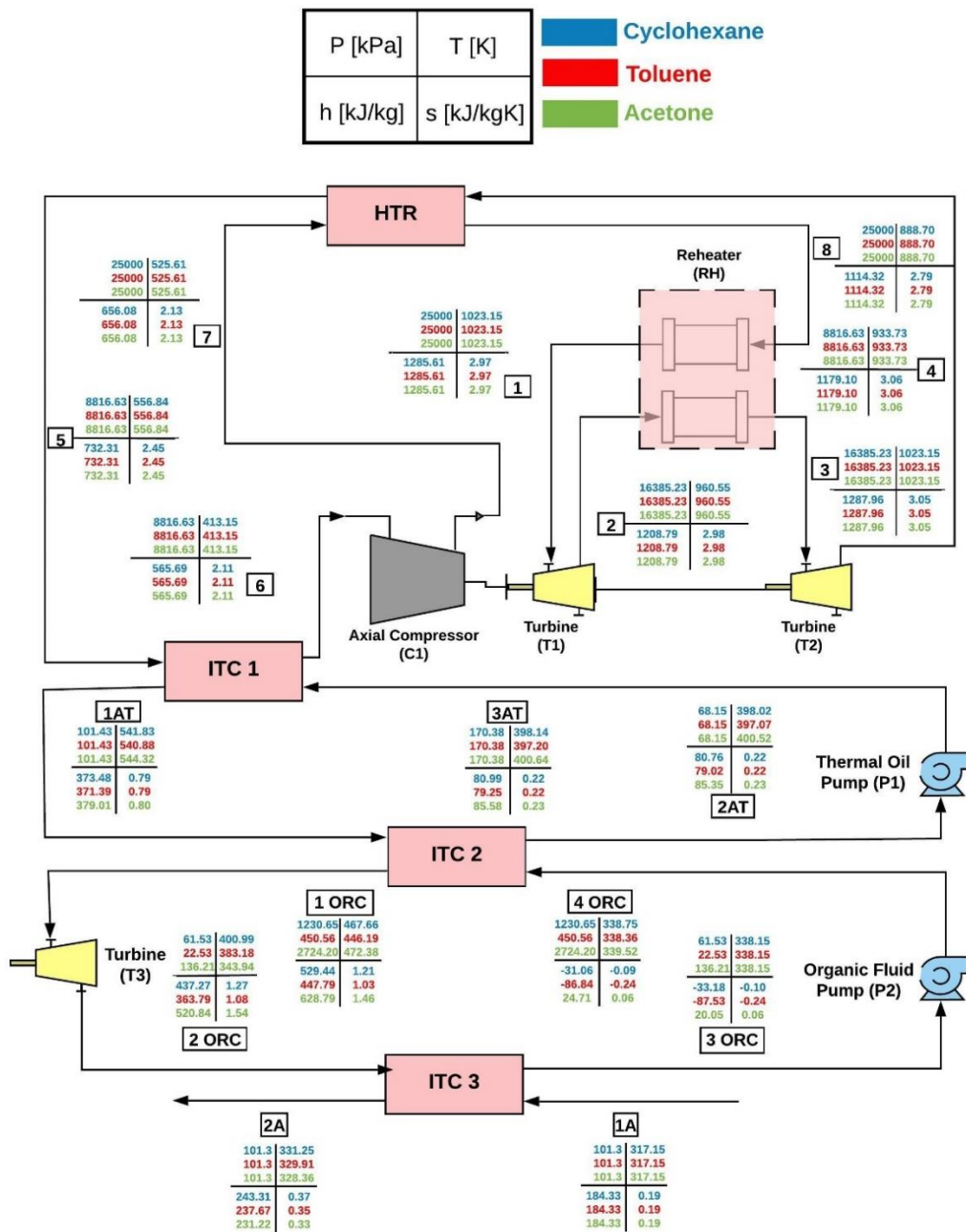


Figure 1. Physical structure of the Brayton S-CO₂ integrated into an organic Rankine cycle (ORC) as a bottoming cycle.

2.2. Working Fluids Properties

To determine the thermodynamic properties in the ORC cycle, the types of fluids used in the system are determined through the T-s diagram (Figure 2). The working fluids are categorized in this diagram according to the slope of the saturation vapor line, and it is known that the dry fluid displays a positive slope in the diagram, a negative slope in the wet fluids, and an extremely broad slope in the isentropic fluids.

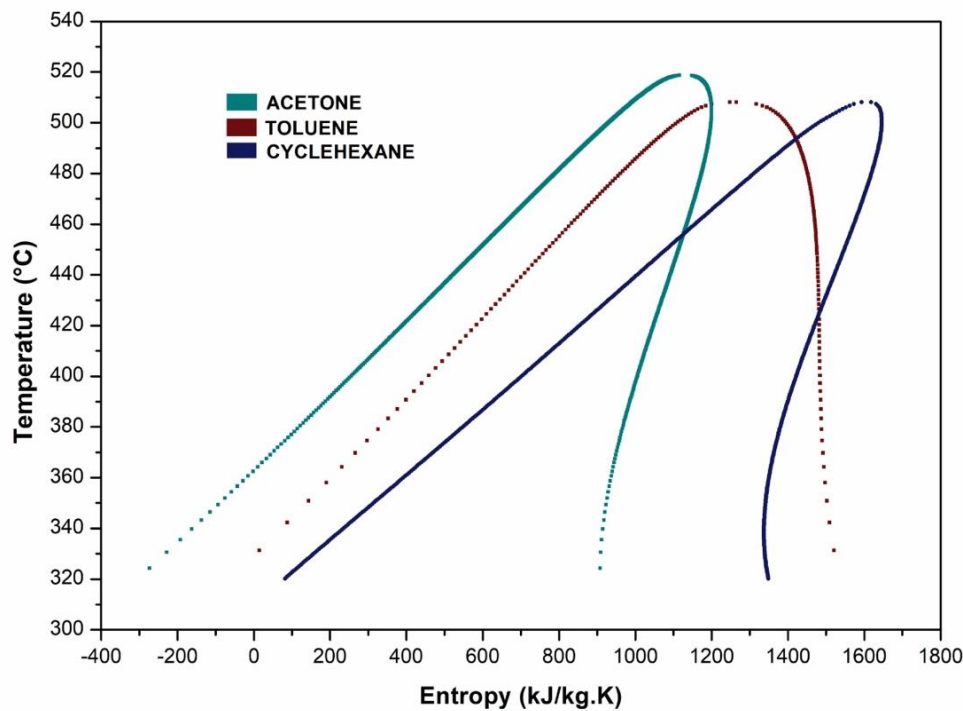


Figure 2. Entropy Temperature (T-s) diagram of organic fluids.

According to Equation (1), the fluid type is defined based on the slope of the saturation line. This slope classifies the working fluids by value of $E = \frac{\partial s}{\partial T}$ obtaining for dry fluids $E > 0$ isentropic fluids, $E \approx 0$, and wet fluids $E < 0$ [37].

$$E = \frac{C_p}{T_H} - \frac{n \cdot T_H - T_{rH} + 1}{T_H^2 \cdot (1 - T_{rH})} \Delta H_H \quad (1)$$

where $T_{rH} = \frac{T_H}{T_C}$, and ΔH_H is the enthalpy of evaporation.

2.3. Thermodynamic Analysis

The consideration adopted for carrying out the combined Brayton S-CO₂ and ORC thermodynamic modeling are listed below [29]:

- The components were assumed as open systems in a stable state condition.
- The atmospheric temperature and pressure were set to 25 °C and 101.3 kPa, respectively.
- The kinetic and potential energy was not considered in the energy balance.
- The Brayton-CO₂ compressor is studied under similar turbine conditions.
- The consequences of pressure fluctuations are not known.
- Pressure drops in the tubing are not known.
- Pressure drops in structure heat exchangers are estimated depending on the geometry and flow regime characteristics.

The energy balance in steady-state for the devices is presented in Equation (2)

$$\dot{Q} - \dot{W} + \sum \dot{m}_{in} \cdot h_{in} - \sum \dot{m}_{out} \cdot h_{out} = 0 \quad (2)$$

where \dot{Q} is the heat at the boundary in kW, \dot{W} is the conversion of energy by work in kW, h is the specific enthalpy value for the working fluid in kJ/kg·K, and \dot{m} is the mass flow rate in kg/s.

To calculate the working fluid exergy as a function of the ambient conditions, Equation (3) is used.

$$e_i = h_i - h_0 + T_0 s_0 - T_0 s_i \quad (3)$$

For each device of the cycle, the exergy destruction can be determined with the exergy balance described in Equation (4)

$$\dot{E}D_{di} = \dot{E}D_{Q_i} - \dot{E}D_{W_i} + \sum \dot{m}_{in} \cdot e_{in} - \sum \dot{m}_{out} \cdot e_{out} \quad (4)$$

where $\dot{E}D_{di}$ is the exergy destruction rate for components (i), the exergy rate by work and heat movement over the boundary is $\dot{E}D_{W_i}$ and $\dot{E}D_{Q_i}$, and the inlet and outlet related exergy rates are e_{in} and e_{out} .

The exergy rate by heat transfer is determined with Equation (5)

$$\dot{E}D_{Q_i} = \dot{Q}_i \cdot \left(1 - \frac{T_0}{T_s}\right) \quad (5)$$

where T_0 is the atmospheric temperature, and T_s is the source temperature if the heat is produced and the temperature decreases when the heat is lost in the system. Also, Equation (6) is often used to quantify the exergy destruction rate by component ($\dot{E}D_{di}$)

$$\dot{E}D_{di} = T_0 \cdot \dot{s}_{gen.i} \quad (6)$$

where $\dot{s}_{gen.i}$ is the rate of entropy production, which is calculated with the general entropy balance with Equation (7), as shown as follows:

$$\dot{s}_{gen.i} = \sum \dot{m}_{out} \cdot s_{out} - \sum \dot{m}_{in} \cdot s_{in} - \sum \frac{\dot{Q}}{T} \quad (7)$$

The net power of the Brayton cycle ($\dot{W}_{net,Brayton\ S-CO_2}$) is calculated based on Equation (8), from the power of the main turbine (T1), the secondary turbine (T2) and the compressor (C1).

$$\dot{W}_{net, Brayton\ S-CO_2} = \dot{W}_{T1} + \dot{W}_{T2} - \dot{W}_{C1} \quad (8)$$

Equation (9) determines the net power of the ORC cycle ($\dot{W}_{net,ORC}$), based on the power of the turbine (T3) and pumps (P1 and P2).

$$\dot{W}_{net,ORC} = \dot{W}_{T3} - \dot{W}_{P1} - \dot{W}_{P2} \quad (9)$$

The ORC thermal efficiency ($\eta_{I,ORC}$) can be written based on Equation (10).

$$\eta_{I,ORC} = \frac{\dot{W}_{net,ORC}}{\dot{Q}_{ITC1}} \quad (10)$$

where $\dot{W}_{net,ORC}$ is the net power of the ORC, and \dot{Q}_{ITC1} is the heat collected from the heat exchanger.

Equation (11) is used to calculate the thermal performance of the Brayton cycle as a function of the net power of the Brayton cycle and the heat received from the thermal source (\dot{Q}_{RH}).

$$\eta_{I,Brayton\ S-CO_2} = \frac{\dot{W}_{net,Brayton\ S-CO_2}}{\dot{Q}_{RH}} \quad (11)$$

Also, considering the second law of thermodynamics, the exergy efficiency ($\eta_{II,ORC-Brayton\ S-CO_2}$) is calculated, as shown in Equation (12)

$$\eta_{II,ORC-Brayton\ S-CO_2} = \frac{\dot{E}D_{prod}}{\dot{E}D_{fuel}} \quad (12)$$

where $\dot{E}D_{fuel}$ and $\dot{E}D_{prod}$ are the fuel and product exergy rate for the components, which are defined in Table 1.

Table 1. Fuel-Product definition for the ORC and Brayton S-CO₂ components.

Cycle	Equipment	Fuel	Product	Loss
ORC	ITC1	\dot{E}_5	$\dot{E}_{1AT} - \dot{E}_{3AT}$	-
	P1	\dot{W}_{P1}	$\dot{E}_{3AT} - \dot{E}_{2AT}$	-
	ITC2	$\dot{E}_{1AT} - \dot{E}_{2AT}$	$\dot{E}_{1ORC} - \dot{E}_{4ORC}$	-
	T3	$\dot{E}_{1ORC} - \dot{E}_{2ORC}$	\dot{W}_{T1}	-
	ITC3	-	-	\dot{E}_{2A}
	P2	\dot{W}_{P2}	$\dot{E}_{4ORC} - \dot{E}_{3ORC}$	-
Brayton S-CO ₂	C1	\dot{W}_{comp}	$\dot{E}_7 - \dot{E}_6$	-
	T1	$\dot{E}_1 - \dot{E}_2$	\dot{W}_{t1}	-
	T2	$\dot{E}_3 - \dot{E}_4$	\dot{W}_{t2}	-
	RH	$\dot{E}_8 - \dot{E}_1 + \dot{Q}_s$	$\dot{E}_3 - \dot{E}_2$	-
	HTR	$\dot{E}_4 - \dot{E}_5$	$\dot{E}_8 - \dot{E}_7$	-
	C1	\dot{W}_{comp}	$\dot{E}_7 - \dot{E}_6$	-

Thus, the overall thermal efficiency of the integrated system Brayton S-CO₂-ORC is a function of net power and heat source, as shown in Equation (13).

$$\eta_{I,overall} = \frac{\dot{W}_{net,Brayton\ S-CO_2} + \dot{W}_{net,ORC}}{\dot{Q}_{RH}} \quad (13)$$

2.4. LCA in the Brayton S-CO₂-ORC System

The LCA procedure was adopted to investigate the potential environmental impacts of the components and organic fluids of the *Brayton S-CO₂-ORC* in each phase of the life cycle. This procedure is developed according to the ISO 140009 environmental management standards and is supplemented by some steps such as definition, inventory, life cycle impact assessment analysis, results, and interpretation [38].

This analysis was applied in the Barranquilla city (Colombia) in the year 2020. The suggested practical unit is 1 kWh produced by the *Brayton S-CO₂-ORC* system, while the scope of the analysis considers the assembling procedures of materials and divisions of the cycle (construction phase). Also, the operation and maintenance phase was considered as a function of the energy ratio of the equipment. The decommissioning period of the system is likewise considered in the LCA of the thermal system, as shown in Figure 3.

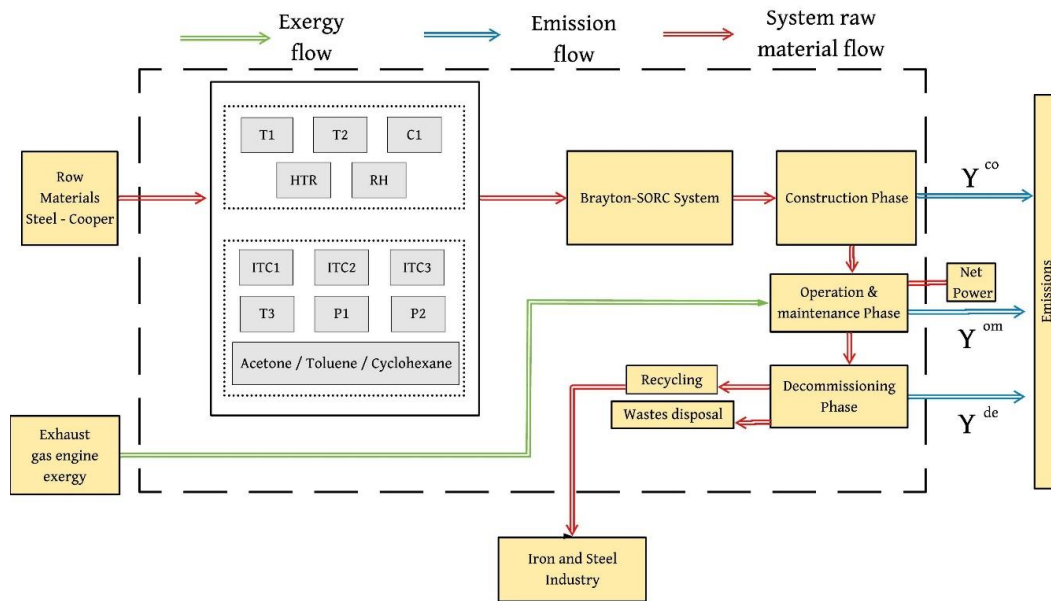


Figure 3. Life cycle assessment system boundary diagram.

Some considerations were adopted to conduct the LCA, such as the Eco-indicator 99 approach, which was utilized in [38]. The environmental impact of the organic working fluid, the components, and the thermal oil are considered in the three phases of the process lifecycle, which are the construction, operation, and maintenance and decommissioning [39]. The normal loss of organic working fluid in an ORC ranges from 0 to 2% of the total filled fluid. So, for a period of 20 years, the working fluid loss considered was 0.5%. As needs are, the liquid loss in the operation phase is 10%, while the organic loss in the decommissioning stage is just 3%. Also, it was assumed that the composition of the thermal oil (Therminol) is 73.5% Diphenyl Oxide for the environmental impact assessment of the thermal oil. Concerning the toxicity of working fluids, in the selection of these, it has been recommended to use nontoxic and nonflammable organic fluids. Therefore, only fluids with classifications A1, B1, A2L, B2L were selected, under ASHRAE standard 34-2001 or the NFPA 704 standard [40,41].

By applying the energy balance in the heat exchangers (ITC1, ITC2, and ITC3), the heat transfer area is obtained with Equation (14)

$$A_i = \frac{\dot{Q}}{\Delta t} \cdot \frac{1}{U} \quad (14)$$

where U is the heat transfer coefficient in $\text{kW/m}^2 \cdot \text{K}$, and Δt is the true temperature difference, determined with the Equation (15)

$$\Delta t = CF_T \cdot LTD \quad (15)$$

where CF_T is the correction factor calculated with the Equation (16), and LTD is the logarithmic mean temperature differences calculated according to Equation (17) [42]

$$CF_T = \frac{\frac{\sqrt{R^2+1}}{R-1} \cdot [\ln(1-S) - \ln(1-RS)]}{\ln \frac{2-S \cdot (R+1 - \sqrt{R^2+1})}{2-S \cdot (R+1 + \sqrt{R^2+1})}} \quad (16)$$

$$LTD = \frac{\Delta T_{10-1AT} - \Delta T_{11-3AT}}{\ln \left(\frac{\Delta T_{10-1AT}}{\Delta T_{11-3AT}} \right)} \quad (17)$$

where R corresponds to the effectiveness coefficient, and S is the heat power ratio.

The modeling of the printed circuit heat exchangers is carried out according to the mathematical model presented in the literature [31]. This heat exchanger is the Recuperator (HTR) and the Reheater

(RH) in the Brayton cycle, which are fabricated by such technologies as chemical etching and diffusion bonding, where flow channels are imprinted chemically on the metal plates and produce one block by diffusion adhering, as shown in Figure 4.

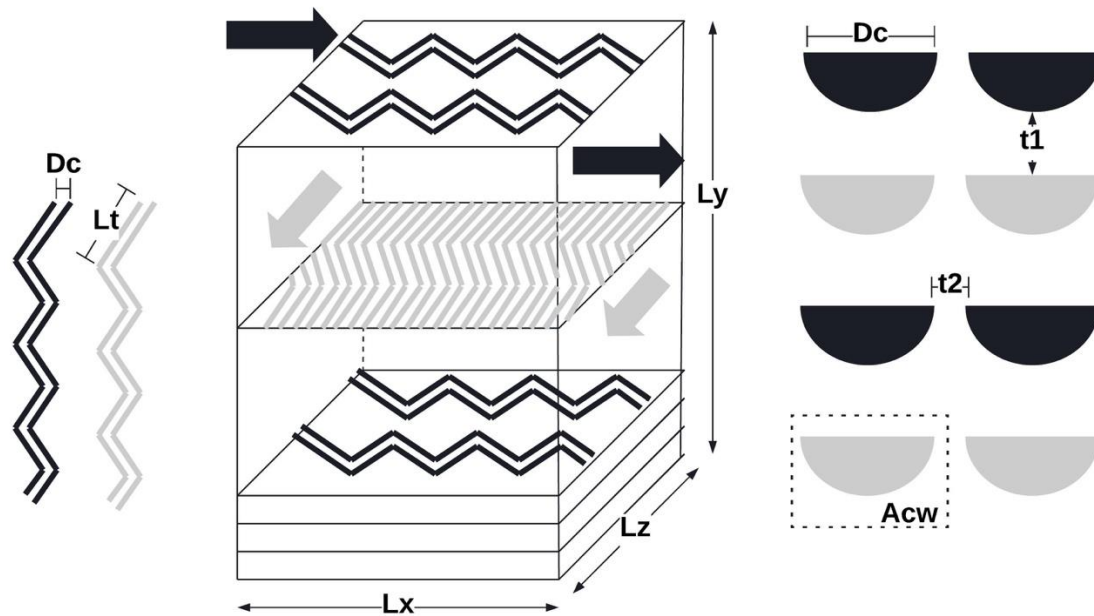


Figure 4. Printed circuit heat exchangers geometrical design.

The heat exchanger is calculated by dividing it into small sub-exchangers (Equation (18)) in which the properties of the fluid, temperature, and pressure are known, and an iterative process is followed until both the heat exchanged and the maximum pressure drop are satisfied. The correlations used for each of the *i* divisions were obtained from the literature [31]

$$N_{UI} = \begin{cases} 4.089 & \text{if } Re_i < 2300 \\ 4.089 + \frac{Nu_{5000} - 4.089}{5000 - 2300} \cdot (Re_i - 2300) & \text{if } 2300 < Re_i < 5000 \\ \frac{\left(\frac{f_i}{8}\right) \cdot (Re_i - 1000) \cdot Pr_i}{1 + 12.7 \cdot (Pr_i^{\frac{2}{3}} - 1) \cdot \sqrt{\frac{f_i}{8}}} & \text{if } Re_i > 5000 \end{cases} \quad (18)$$

where *f* is the Darcy factor and *Pr* is the Prandtl number.

The heat transfer coefficient is then calculated using Equation (19)

$$H_i = N_{UI} \cdot (k/D_{hid}) \quad (19)$$

where *k* is the conductivity of the exchanger material [W/m·K].

Finally, the overall coefficient *U* of each element is calculated using Equation (20), and the length of each of the sub-exchangers with Equation (21).

$$U_i = \frac{1}{\frac{1}{H_{hi}} + \frac{1}{H_{ci}} + \frac{t}{k}} \quad (20)$$

$$L_i = \frac{Q_i}{P_i \cdot Q_i \cdot (T_{hm} - T_{cm})} \quad (21)$$

where *t* is the thickness of the plate, and *P_i* is the wet parameter.

When calculating the heat exchanger, you check that it meets the introduced pressure drop using Equation (22).

$$\Delta P_i = f_i \cdot \left(\frac{L_i}{D_{hid_i}} \right) \cdot \left(\frac{c_i^2}{2} \right) \quad (22)$$

The heat exchanger mass can be calculated using Equation (23)

$$M_i = \rho \cdot A_i \cdot \delta \quad (23)$$

where ρ is the density (steel is 7930 kg/m³, and copper is 8900 kg/m³), and δ is the material thickness with a value of 0.002 m [32].

The turbine and pump masses are determined using Equation (24)

$$M_i = \alpha \cdot W_i \quad (24)$$

where W_i is the turbine power produced, or the pump power consumed α is the required quality of the material in kg/kW. For steel, the value for α is 14 kg/kW and 31.22 kg/kW for the pump and the turbine, respectively, while for copper, its value is 35.03 kg/kW and 15.71 kg/kW for the turbine and the pump, respectively [32].

According to Equation (25), the environmental impact of each equipment can be described

$$Y_i = w_i \cdot M_i \quad (25)$$

where w_i is the component coefficient Eco 99.

Therefore, the environmental impact of equipment (Y^{LCA}_k) is obtained using Equation (26) [43]

$$Y^{LCA}_i = Y^{co}_i + Y^{om}_i + Y^{de}_i \quad (26)$$

where Y^{co}_i , Y^{om}_i and Y^{de}_i lead to the environmental impacts of the corresponding phases: construction, operation, and decommissioning.

Finally, the total environmental impacts of components are determined with Equation (27)

$$Y_i = Y^{LCA}_i + Y^{wf}_i \quad (27)$$

where Y^{wf}_i is the effect of the organic fluid volume used in each component, and is a function of the component's exergy destruction, which is determined using Equation (28).

$$Y^{wf}_i = \frac{Y^{wf} \cdot \dot{E}D_{di}}{\dot{E}D_{d-total}} \quad (28)$$

3. Results and Discussion

3.1. System Thermodynamic and Exergy Performance

Figure 5 shows a sensitivity analysis of the thermodynamic and exergy performance indicators of the thermal cycle, based on the inlet temperature of the main turbine (T1) in the Brayton S-CO₂-ORC configuration. For the development of the sensitivity analysis, the following considerations were taken into account ORC pressure ratio was 30, evaporator pinch point 25 °C, main turbine inlet temperature (TIT) 750K, Brayton cycle high pressure 25 kPa, Brayton turbine efficiency 93%, ORC turbine 80%, compressor efficiency 89%, pump efficiency 75%, and HTR effectiveness 95%. Figure 5a shows the net power generated with the different organic working fluids simulated in the system, observing that as the temperature increases there is a 36% increase in the net power delivered by the system for a range between 550 °C and 800 °C, showing similar trends among the three organic working fluids studied.

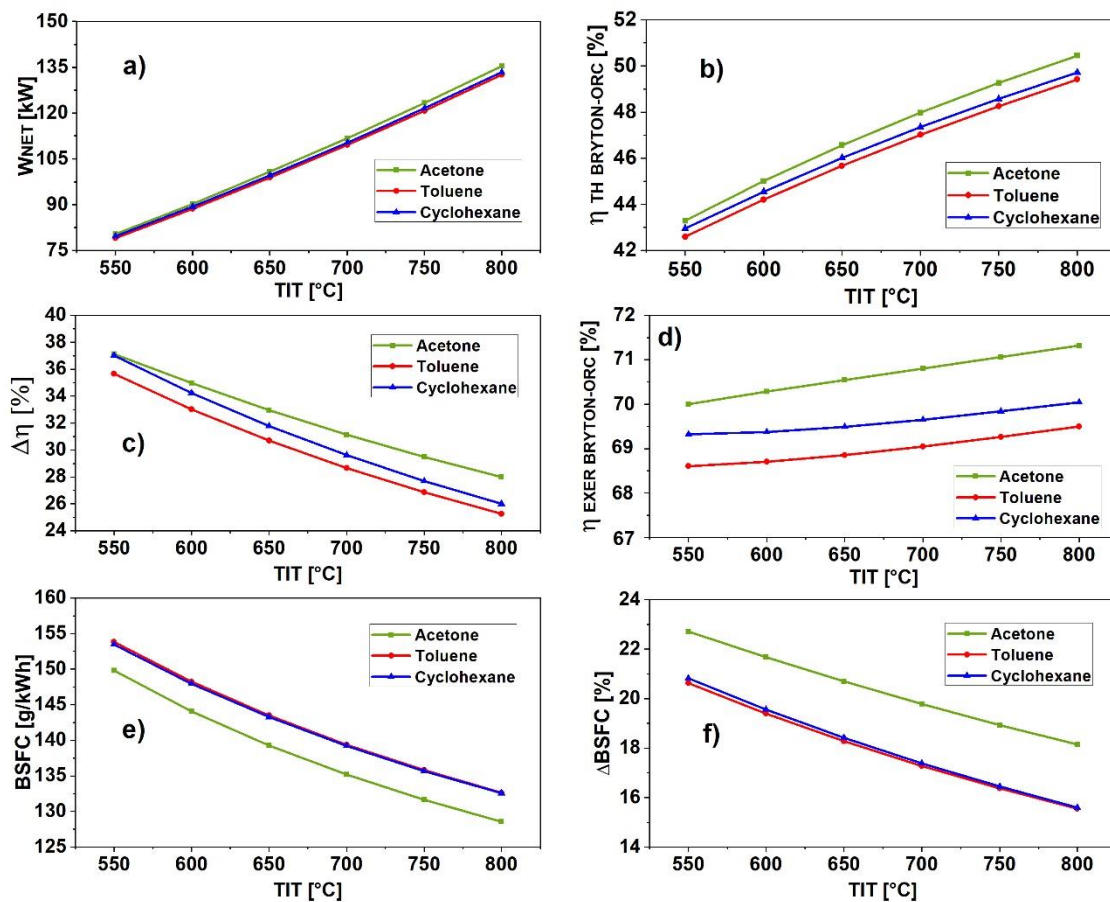


Figure 5. System performance parameters with respect to TIT, (a) net power; (b) thermal efficiency Brayton-ORC; (c) absolute increase in thermal efficiency; (d) exergy efficiency Brayton-ORC; (e) brake-specific fuel consumption; (f) absolute decrease in brake-specific fuel consumption.

In the case of the thermal efficiency of the Brayton S-CO₂-ORC integrated system, as shown in Figure 5b, acetone is the fluid with the best thermal performance in the operation of the configurations, this is because its thermo-physical properties benefit the best use of energy and the performance of the system components, reaching a maximum thermal efficiency of 50.44% at 800 °C, this being the best operating condition of this fluid. Therefore, each fluid presents its particular operating conditions that must be studied to optimize the energetic, exergetic, and environmental performance of each proposed alternative [33,34].

Figure 5d shows the total exergetic efficiency of the system studied, where the turbine T1 inlet temperature has a positive influence on all the organic working fluids studied. Toluene and cyclohexane exhibited similar behavior. However, acetone exceeds an exergetic efficiency of 71.4% at a turbine inlet temperature of 800 °C. Through the analysis of this parameter, it contributes to the objective of making more effective use of the nonrenewable energy resource used in the Brayton cycle by establishing the components, modes, and actual amounts of exergy destruction and loss in the integrated system. The values obtained for exergetic efficiency are of great importance in this study since they allow for the design of a more effective integrated Brayton S-CO₂-ORC configuration, aimed at the reduction of inefficiencies in these systems. The acetone presented the best average behavior among the fluids in the temperature range studied, concerning toluene and cyclohexane, with a difference of 2.9% and 2.7%, respectively, which is a consequence of the thermal properties of this fluid. However, before implementing these results at the industrial level, advanced economic analyses and exertion of these systems must be carried out [35], in addition to thermo-economic studies to determine the technical and economic feasibility of this solution [36].

The high turbine pressure in the system is another relevant operational parameter that impacts on the energy and exergy efficiency of the integrated system; however, this variable has less impact than the main turbine inlet temperature (T_1), producing less variability in the performance parameters, as can be seen in Figure 6. For the performance of the net power, it presents less efficiency in its behavior concerning the performance affected by the inlet temperature (Figure 5a), presenting an approximate increase of 36% beside 9% of the energy generated by the system.

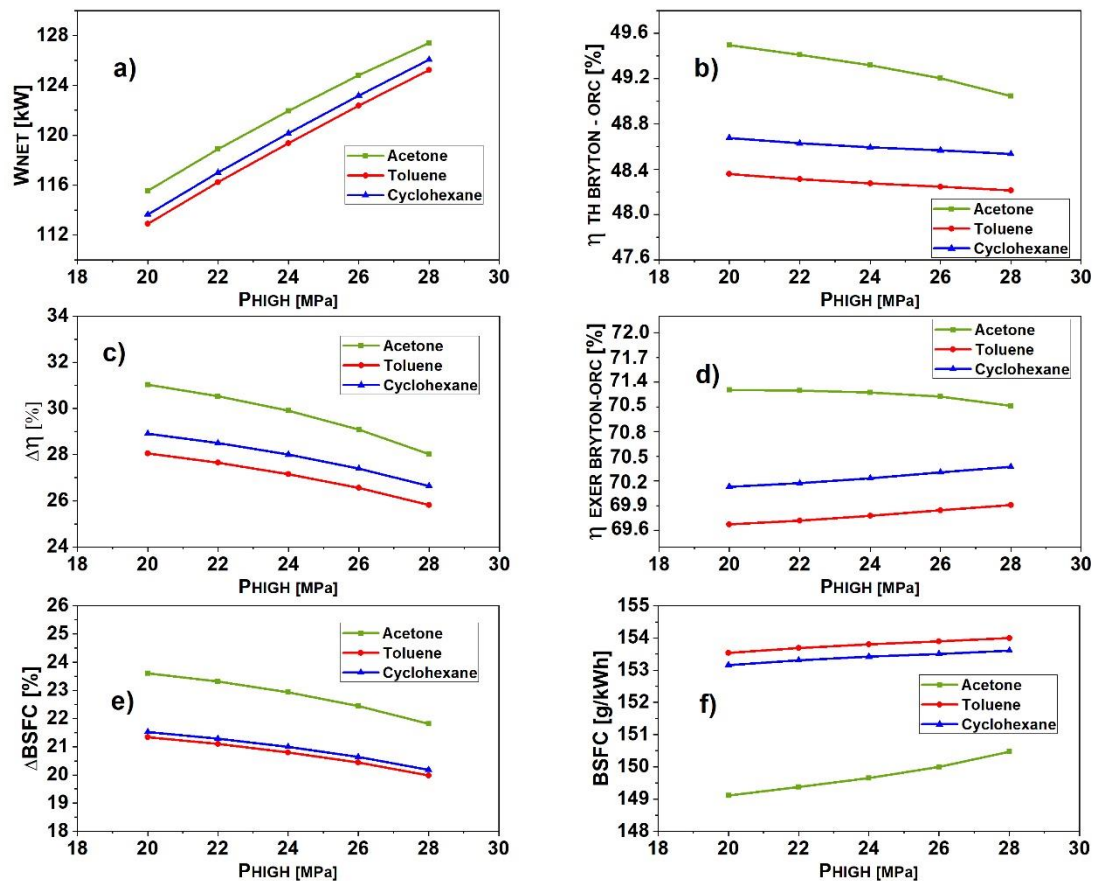


Figure 6. System performance parameters with respect to P_{HIGH} , (a) net power; (b) thermal efficiency Brayton-ORC; (c) absolute increase in thermal efficiency; (d) exergy efficiency Brayton-ORC; (e) brake-specific fuel consumption; (f) absolute decrease in brake-specific fuel consumption.

On the other hand, Figure 6e shows the decrease in the specific fuel consumption for the three fluids studied in the integrated configuration of the Brayton S-CO₂-ORC system, with acetone showing the best performance of the three fluids due to its better specific consumption reduction. This result is closed near the other parameter calculated. This result implies a significant reduction in the system operating costs. It allows better use of resources, improving its performance between the energy input and the power produced at high temperatures.

The exergetic efficiency behavior for each component of the system under the three organic working fluids is shown in Figure 7. From the results. The lower exergy efficiency is presented in the thermal oil pump (P1), with a 10.98% (Toluene) and 11.06% (Cyclohexane), while the efficiency in the organic fluid pump (P2) was 77.6% for the three fluids. These results are because of the higher-pressure ratios required to pump the thermal oil, which implies higher irreversibilities for heat transfer in this component. Thus, a thermo-hydraulic design should be proposed for both the evaporator (ITC2) and the shell and tube heat exchanger (ITC1) with the lowest pressure drop, and highest heat transfer.

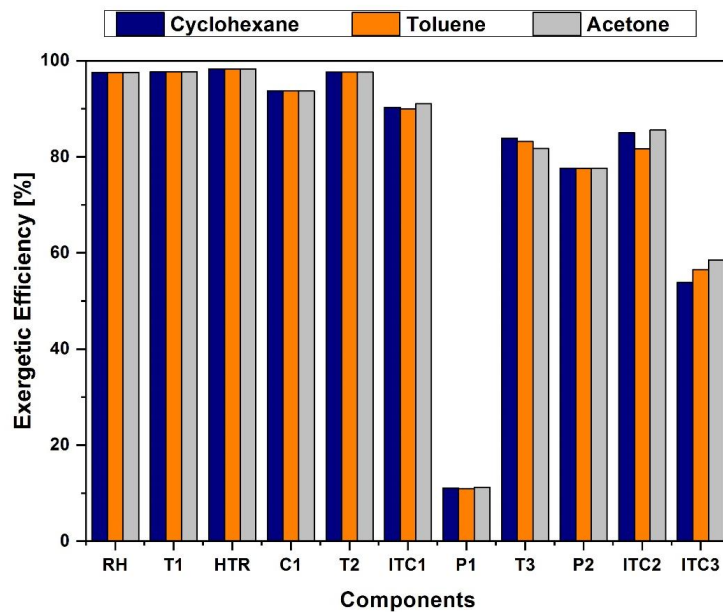


Figure 7. Exergetic efficiency of the Brayton S-CO₂-ORC components.

For the operating conditions studied, the turbine 1 (T1) and the turbine (T2) are the components that present the best behavior, presenting exergetic efficiencies of 98% in the three fluids used to analyze this configuration. Therefore, they present minor irreversibilities and allow better use of the energy in the system.

3.2. Exergy Destruction

To develop an exergy destruction analysis of the system, it was necessary to apply the exergy balance for each of the components as shown in Figure 8, where the exergy destruction fraction of each component is evaluated at different inlet turbine temperature ranging from 550 °C to 800 °C. For this analysis, the operational considerations in Section 3.1 have been taken to determine exergy destruction. The component with the minimum exergy destroyed is the pump (P2) compared to the heat exchanger components that have the greatest exergy destruction in the system. Thus, the ITC2, which is the component with the greatest exergy destroyed with values ranging from 3.93 kW to 9.75 kW for the temperature range evaluated, showing a decrease between the value of exergy destroyed from the base condition of 11% and an increase in exergy destroyed at the temperature of 800 °C of 3%. Although technological improvements do not translate into significant improvements in exergetic efficiency, this result can be improved if ITC1 is designed with rational energy use and sustainability criteria, that leads to sensible improvements in how heat transfer is performed in this type of exchanger, with the aim to obtain more compact, economical and efficient equipment.

The thermal oil pump (P1), and the organic fluid pump (P2) were the components that presented minimum exergy destruction. An alternative to having equipment with less exergy destruction would be to propose pumping systems with higher exergy efficiency, which would imply an increase in the net power produced by the cycle because the pump will consume less energy. However, the pump power is less than that produced by the turbine, which is the reason for the lower contribution of the exergy destroyed and the isentropic efficiency on the overall thermal cycle performance, as the contribution of these is almost indistinguishable when compared with the exergy destroyed from the other components of the cycle at the different inlet turbine temperatures.

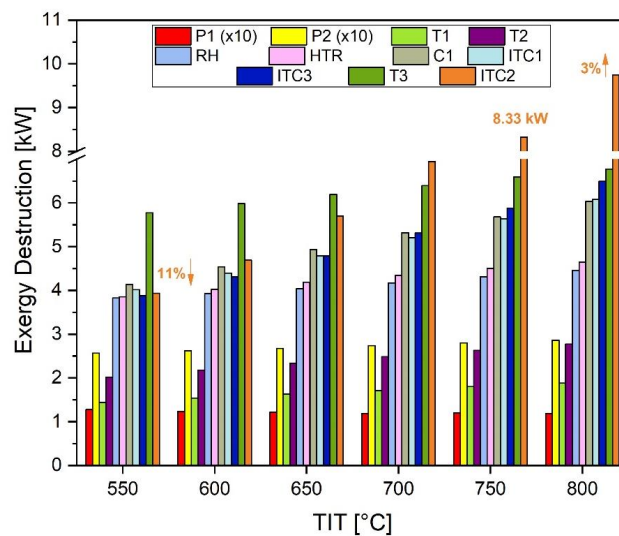


Figure 8. Components destroyed exergy with respect to turbine inlet temperature (TIT).

The influence of the P_{HIGH} on the destroyed exergy by components is presented in Figure 9, where the ITC2 is the component with the highest irreversibility in the configuration studied. This trend of the exergy destruction continues as the high-pressure turbine decreases, obtaining approximately 8.67 kW of exergy destroyed in the system by this component when the pressure is 20 MPa, which is reflected in a significant energy loss in this component due to the large size of this heat exchanger. Therefore, the operating conditions in the Brayton cycle at the input of operation, although it makes the cycle deliver more power, at the time of coupling with ORC cycle, show important irreversibilities by heat transfer in the thermal circuit of coupling due to operational limitations to ensure thermal stability on the thermal oil and organic fluid. These results can be compared with the results made by the authors in the following references, where they use other working fluids and different models and heat recovery systems [44,45].

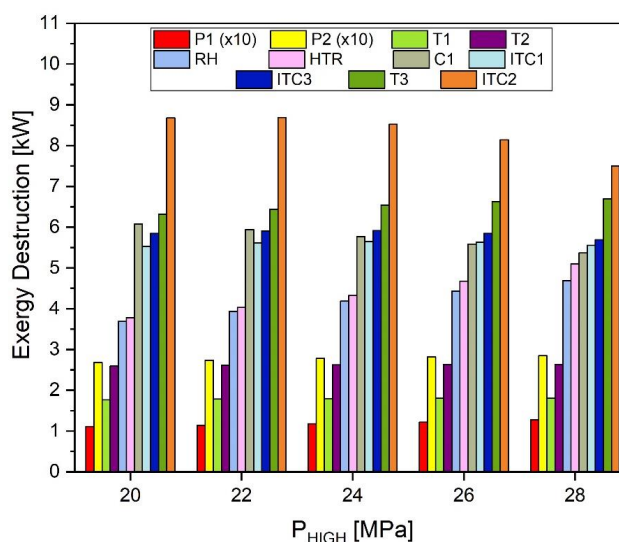


Figure 9. Components destroyed exergy with respect to P_{HIGH} .

Similarly, the exergy destruction in the HTR used in the system increases as the P_{HIGH} increases from 20 MPa to 28 MPa, being this the second component with more impact in the process, reaching a value of 5.10 kW in the exergy destruction at the maximum operating condition. These results are due to the presence of greater irreversibilities in the thermal source, as it is required that the organic working fluid reaches a higher pressure and temperature; therefore, this variable must be considered

as an objective variable in energy and exergetic optimization to obtain competitive efficiencies for the system operating with the energy source under study.

3.3. Life Cycle Assessment

Based on the thermodynamic parameters of each state of the Brayton S-CO₂-ORC integrated system, the energy and exergetic parameters of the organic components and organic fluids are shown in Table 2. In the proposed system, a lifetime of 20 years was considered [46], in which the components and working fluids will have 7446 working hours [47,48].

Table 2. Exergy efficiency, destroyed exergy, destroyed exergy ratio of each equipment, and heat exchanger area.

Parameter	ITC 1			ITC2		
	Cyclohexane	Toluene	Acetone	Cyclohexane	Toluene	Acetone
\dot{Q}_i [kW]	182.00	166.62	181.84	165.08	165.08	165.08
A_i [m ²]	88.70	88.70	88.70	18.73	16.86	17.51
ε_i [%]	90.27	89.96	91.08	85.02	81.71	85.54
$\dot{E}D_k$ [kW]	6.15	5.17	5.64	8.55	10.41	8.33
$y_{D,k}$ [%]	13.15	11.09	12.32	18.28	22.32	18.20
Parameter	ITC3					
	Cyclohexane		Acetone	Toluene		Acetone
\dot{Q}_i [kW]	138.56			139.36		136.86
A_i [m ²]	10.06			8.58		6.46
ε_i [%]	53.85			56.53		58.52
$\dot{E}D_k$ [kW]	7.69			6.74		5.88
$y_{D,k}$ [%]	16.44			14.44		12.86
Parameter	RHR			HTR		
	Cyclohexane	Toluene	Acetone	Cyclohexane	Toluene	Acetone
\dot{Q}_i [kW]	250.46	250.46	250.46	446.79	446.79	446.79
A_i [m ²]	176.24	176.24	176.24	15.66	15.66	15.66
ε_i [%]	97.57	97.57	97.57	98.30	98.30	98.30
$\dot{E}D_k$ [kW]	4.31	4.31	4.31	4.50	4.50	4.50
$y_{D,k}$ [%]	9.21	9.25	9.42	9.61	9.65	9.83
Parameter	T1			T2		
	Cyclohexane	Toluene	Acetone	Cyclohexane	Toluene	Acetone
\dot{W}_i [kW]	76.82	76.82	76.82	108.86	108.86	108.86
ε_i [%]	97.71	97.71	97.71	97.64	97.64	97.64
$\dot{E}D_k$ [kW]	1.80	1.80	1.80	2.63	2.63	2.63
$y_{D,k}$ [%]	3.84	3.86	3.93	5.61	5.63	5.74
Parameter	T3			C1		
	Cyclohexane	Toluene	Acetone	Cyclohexane	Toluene	Acetone
\dot{W}_i [kW]	27.15	25.94	29.50	90.39	90.39	90.39
ε_i [%]	83.88	83.22	81.74	93.72	93.72	93.72
$\dot{E}D_k$ [kW]	5.22	5.23	6.59	5.68	5.68	5.68
$y_{D,k}$ [%]	11.14	11.21	14.40	12.14	12.18	12.41
Parameter	P1			P2		
	Cyclohexane	Toluene	Acetone	Cyclohexane	Toluene	Acetone
\dot{W}_i [kW]	0.14	0.14	0.14	0.62	0.21	1.27
ε_i [%]	11.06	10.98	11.25	77.62	77.60	77.66
$\dot{E}D_k$ [kW]	0.13	0.13	0.12	0.14	0.05	0.28
$y_{D,k}$ [%]	0.27	0.27	0.27	0.30	0.10	0.62
Brayton S-CO ₂ -ORC						
Parameter	Cyclohexane		Acetone	Toluene		Acetone
\dot{W}_{net} [kW]	121.67			120.87		123.38
$\eta_{I,Brayton\ S-CO_2-ORC}$ [%]	48.58			48.26		49.26
$\Delta\eta$ [%]	27.70			26.86		29.49
$\eta_{II,Brayton\ S-CO_2-ORC}$ [%]	70.27			69.81		71.25

The results allow for identifying that the RHR is one of the components that presents greater environmental impacts due to their heat transfer area in comparison with the rest of the components of the system. Also, the RHR presents the greatest exergy destroyed, with values of 46% (cyclohexane), 32% (toluene), and 32% (acetone).

The masses in the different phases of the life cycle of the Brayton S-CO₂-ORC system are presented in Table 3. The LCA methodology was developed to obtain the environmental impacts of each component of the system under the three phases of the lifetime, which are the construction, operation and decommissioning, as shown in Table 4, selecting steel as the material. Table A1 shows the results when copper is proposed as the construction material for the devices.

Table 3. Organic fluids and thermal oil masses in each life cycle phase.

Fluid	LCA Phase		
	Construction	Operation	Decommissioning
Cyclohexane	151.2078	15.1208	4.0826
Toluene	144.4687	14.4469	3.9007
Acetone	164.3074	16.4307	4.4363
Thermal Oil	184.4000	18.44	4.9788

Table 4. Results of Life Cycle Assessment for each component selecting steel as the material.

Organic Fluid	Equipment	Material	w [mPts/kg]	Quality [kg]	Y ^{co} [mPts]	Y ^{om} [mPts]	Y ^{de} [mPts]	Y [mPts]
Cyclohexane	ITC1	Steel	86	1407	127,037	0	6049	133,086
	ITC2	Steel	86	297	26,823	0	1277	28,100
	ITC3	Steel	86	159	14,402	0	686	15,088
	RHR	Steel	86	2795	252,404	0	12,019	264,423
	HTR	Steel	86	248	22,428	0	1068	23,496
	T1	Steel	86	2398	216,579	0	10,313	226,893
	T2	Steel	86	3399	306,903	0	14,614	321,518
	T3	Steel	86	848	76,531	0	3644	80,176
	C1	Steel	86	2822	254,838	0	12,135	266,973
	P1	Steel	86	2	178	0	8	186
	P2	Steel	86	9	789	0	38	826
	Thermal Oil Fluid	Therminol Cyclohexane	46,467 2639	184 151	856,8515 399,022	856,851 39,902	231,350 10,774	9,656,716 449,698
Toluene	ITC1	Steel	86	1407	127,037	0	6049	133,086
	ITC2	Steel	86	267	24,139	1	1149	25,290
	ITC3	Steel	86	136	12,291	2	585	12,879
	RHR	Steel	86	2795	252,404	3	12,019	264,426
	HTR	Steel	86	248	22,428	4	1068	23,500
	T1	Steel	86	2398	216,579	5	10,313	226,898
	T2	Steel	86	3399	306,903	6	14,614	321,524
	T3	Steel	86	810	73,121	7	3482	76,609
	C1	Steel	86	2822	254,838	8	12,135	266,981
	P1	Steel	86	2	178	9	8	195
	P2	Steel	86	3	270	10	13	293
	Thermal Oil Fluid	Therminol Toluene	46,467 2680	184 144	8,568,515 387,147	856,851 10,941	231,350 10,453	9,656,716 408,541
Acetone	ITC1	Steel	86	1407	127,037	0	6049	133,086
	ITC2	Steel	86	278	25,081	1	1194	26,277
	ITC3	Steel	86	103	9257	2	441	9700
	RHR	Steel	86	2795	252,404	3	12,019	264,426
	HTR	Steel	86	248	22,428	4	1068	23,500
	T1	Steel	86	2398	216,579	5	10,313	226,898
	T2	Steel	86	3399	306,903	6	14,614	321,524
	T3	Steel	86	921	83,162	7	3960	87,129
	C1	Steel	86	2822	254,838	8	12,135	266,981
	P1	Steel	86	2	178	9	8	195
	P2	Steel	86	18	1612	10	77	1699
	Thermal Oil Fluid	Therminol Acetone	46,467 5426	184 164	8,568,515 891,450	856,851 89,145	231,350 24,069	9,656,716 1,004,664

For the three organic working fluids (cyclohexane, toluene, and acetone), the results of the assessment of the environmental impact of the system are presented in Figure 10, where the material of the components is the steel and copper. The components with the greatest environmental impacts are the main turbine (T1) and the secondary turbine T2 of the Brayton S-CO₂ cycle, with values of 226,893 mPts and 321,518 mPts, respectively, when steel is selected as the material. With this, the T1 and T2 turbines obtain, respectively, percentage values of 18.19% and 25.78% (cyclohexane), 20.54% and 29.10% (toluene), 20.36% and 28.85% (acetone). In the ORC, the ITC1 is the component with the greatest environmental impact, with percentage values of 10.67% (cyclohexane), 12.05% (toluene), and 11.94% (acetone) concerning the environmental impacts of all components. When the material is copper, there is a decrease in the percentage values of the T1 and T2 turbines due to the increase in environmental impacts in the ITC1, which obtains values of 11.45% (cyclohexane), 12.85% (toluene) and 12.94% (acetone).

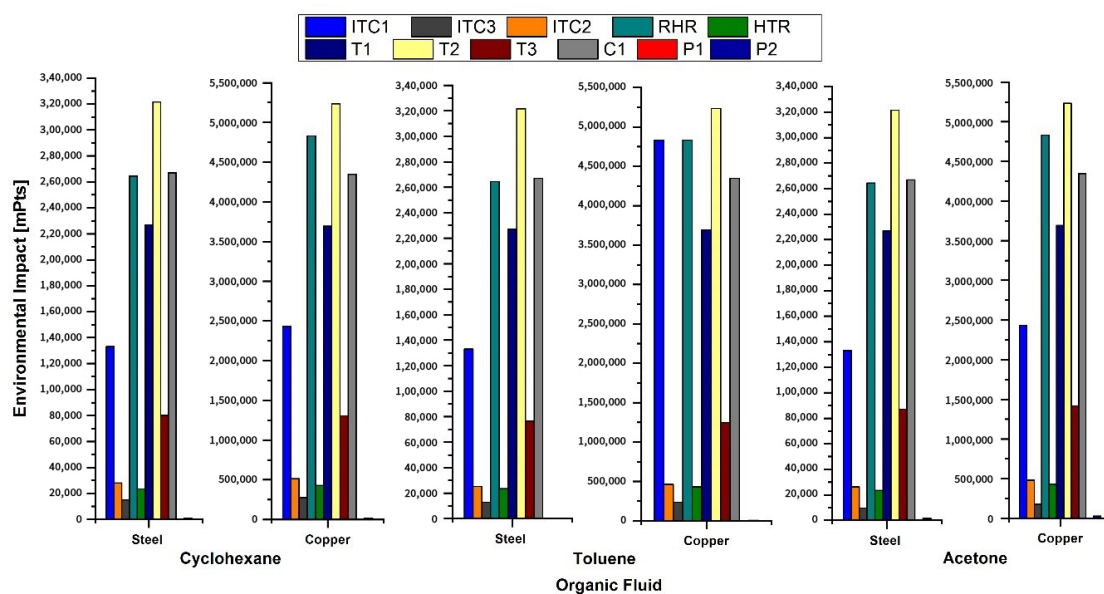


Figure 10. Environmental impact of each equipment with respect to the organic fluids and materials.

In general, the environmental impacts of each equipment when steel is selected as material steel are lower than those of the components with copper because in the methodology applied the Eco99 coefficient is higher than that of steel. Therefore, considering sustainability criteria complementary to the energy and exergetic aspects studied, the organic working fluid and material in which the greatest exergetic opportunities for improvement are found can be selected to obtain the least environmental impact.

Regarding the environmental impacts of working fluids and thermal oil, the results are presented in Figure 11 where the thermal oil has a very large environmental impact on the organic fluids, representing 83% of the environmental impacts compared to cyclohexane (4%), toluene (4%), and acetone (9%), respectively. Among the organic fluids, because it has a higher Eco99 coefficient, acetone has greater environmental impacts than cyclohexane and toluene, and the suggested material is the steel, which is a result close to that reported in the literature for the case of the ORC as heat recovery [37]. Therefore, with the ORC being built with this material and operating with this fluid, it can be widely used for heat recovery from natural gas generation engines [38].

The results show that the greatest differences in LCA are obtained in the environmental impacts in the construction phase, where acetone presents better results for this system, which coincides with the results obtained from the analysis of the energy and exergetic indicators.

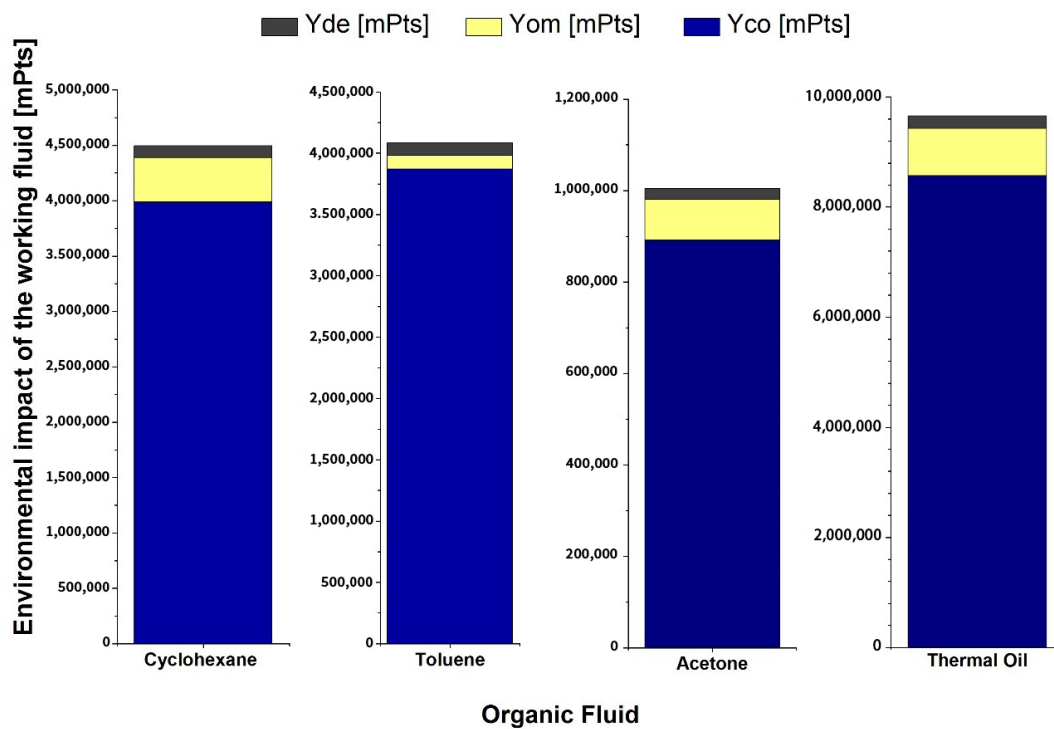


Figure 11. Environmental impact of the working fluid.

4. Conclusions

The main contribution of this study was to analyze the energy, exergy, and environmental performance of an integrated Brayton S-CO₂-ORC, where some performance indicators and the potential environmental impact were studied using Toluene, Acetone, and Cyclohexane as the organic working fluids. Therefore, a complementary assessment was developed based on the energy, exergetic, and environmental analysis to determine the best behavior of the components in this cycle, and the effect of the relevant operating conditions.

For identifying the best performance of the components that integrate this system, the study evaluates exergetic and energy parameters such as the exergetic and overall thermal efficiency under the different organic working fluids used in this study. In these parameters, it is possible to evaluate the power generated by the integrated system for each fluid operating in the Brayton S-CO₂-ORC configuration, where the acetone presented the best behavior with respect to toluene and cyclohexane. The performance of the system for the operating conditions studied found that turbine 1 (T1) and the turbine (T2) are the components that present the best exergetic efficiencies with 97%. Therefore, the acetone offers minor irreversibilities and allows for better performance in the ORC as a bottoming cycle from the Brayton cycle.

Conversely, another relevant parameter studied is the exergy destroyed of each component, presenting the pump (P2) least performance compared to the heat exchanger components that have the most considerable exergy destruction in the system, thus observing that ITC1 is the component with the most exergy destroyed, with values ranging from 75 kW to 127 kW for the temperature range evaluated. So, this component presents greater opportunities for energy improvement, and therefore environmental improvement, since its potential environmental impacts are based on the heat transfer area of this equipment.

For the three working fluids (cyclohexane, toluene and acetone), the results of the potential environmental impacts of the system were studied using the steel and copper as construction materials for the components. The components with the greatest environmental impacts are the main turbine (T1), and the secondary turbine (T2) of the Brayton S-CO₂ cycle, with values of 226 Pts and 321

Pts, respectively. The T1 and T2 turbines obtained a percentage value of 18.19% and 25.78% of the total environmental impact with cyclohexane, 20.54%, and 29.10% with toluene, 20.36% and 28.85% with acetone. Also, the ITC1 in the ORC cycle is the component with the greatest environmental impact, with a percentage value of 10.67% (cyclohexane), 12.05% (toluene) and 11.94% (acetone).

In general, the environmental impacts of the components with steel are lower than those of the components with copper, because the methodology applied suggests a higher Eco99 coefficient than steel. Therefore, through this methodology, the organic working fluid and the material in which the most significant opportunities for improvement are found can be selected to obtain the smallest environmental impact.

Among the organic fluids studied, acetone has lower potential environmental impacts than cyclohexane and toluene, which is a consequence of the Eco99 coefficient. However, some safety and health consideration such be considered to implement the ORC alternative industrially as the bottoming system from the Brayton cycle.

Finally, this study allows for evaluating the performance of the combined cycles for applying this technology in industries for generating energy and net power. Acetone is the fluid with the best thermodynamic and environmental performance results on this configuration because of their thermal properties, giving an option for other studies to proposed an eco-design of this and obtain better exergy and environmental results according to other performance parameters.

Author Contributions: Conceptualization: E.E.B.; Methodology: G.V.O. and J.D.F.; Software: E.E.B., G.V.O., and J.D.F.; Validation: E.E.B., and J.D.F.; Formal Analysis: E.E.B., G.V.O., and J.D.F.; Investigation: E.E.B., G.V.O., and J.D.F.; Resources: G.V.O. and J.D.F.; Writing—Original Draft Preparation: G.V.O.; Writing—Review and Editing: G.V.O. and J.D.F.; Funding Acquisition: G.V.O., and J.D.F. All authors have read and agreed to the published version of the manuscript.

Funding: This work was supported by the Universidad del Atlántico, and Universidad Francisco de Paula Santander in Ocaña - Norte de Santander.

Acknowledgments: This research was supported by the Mechanical Engineering Program of Universidad del Atlántico. The Kai Research Group supports G. Valencia and J. Duarte.

Conflicts of Interest: The authors declare no conflict of interest.

Nomenclature

LCA	Life Cycle Assessment
ORC	Organic Rankine Cycle
\dot{Q}	Heat rate [kW]
\dot{W}	Power [kW]
\dot{m}	Mass flow rate [kg/s]
h	Enthalpy [kJ/kg·K]
s	Specific entropy [kJ/kg·K]
ex	Exergy rate
\dot{E}_D	Exergy destruction rate
η	Efficiency
M	Mass [kg]
A	Area [m ²]
δ	Thickness [m]
CF_T	Correction Factor
Y_i	Environmental Impact [mPts]
Co	Construction
Om	Operation
De	decommissioning
Wf	Working fluid
PPE	Pinch Point of Evaporator

Appendix A

The LCA results in each component of the proposed configurations using copper as the material are presented in Table A1.

Table A1. Results of Life Cycle Assessment for each component selecting copper as the material.

Organic Fluid	Equipment	Material	w [mPts/kg]	Quality [kg]	Y ^{co} [mPts]	Y ^{om} [mPts]	Y ^{de} [mPts]	Y [mPts]
Cyclohexane	ITC1	Copper	1400	1579	2,321,003	0	110,524	2,431,527
	ITC2	Copper	1400	333	490,057	0	23,336	513,393
	ITC3	Copper	1400	179	263,130	0	12,530	275,660
	RHR	Copper	1400	3137	4,611,496	0	219,595	4,831,091
	HTR	Copper	1400	279	409,760	0	19,512	429,272
	T1	Copper	1400	2398	3525712	0	167,891	3,693,603
	T2	Copper	1400	3399	4,996,099	0	237,909	5,234,008
	T3	Copper	1400	848	1,245,860	1	59,327	1,305,187
	C1	Copper	1400	2822	4,148,525	2	197,549	434,6076
	P1	Copper	1400	2	2894	3	138	3035
	P2	Copper	1400	9	12,842	4	612	13,457
	Thermal Oil Fluid	Therminol	Cyclohexane	46,467	184	8,568,515	856,851	231,350
			2639	149	392,031.28	39,203.13	10,585	441,819
Toluene	ITC1	Copper	1400	3137	4,611,495.84	0	219,595	4,831,091
	ITC2	Copper	1400	300	441,035.62	1	21,002	462,038
	ITC3	Copper	1400	153	224,568.70	2	10,694	235,264
	RHR	Copper	1400	3137	4,611,495.84	3	219,595	4,831,094
	HTR	Copper	1400	279	409,759.56	4	19,512	429,276
	T1	Copper	1400	2398	3,525,711.97	5	167,891	3,693,608
	T2	Copper	1400	3399	4,996,098.50	6	237,909	5,234,014
	T3	Copper	1400	810	1,190,334.01	7	56,683	1,247,024
	C1	Copper	1400	2822	4,148,525.01	8	197,549	4,346,082
	P1	Copper	1400	2	2895.92	9	138	3043
	P2	Copper	1400	3	4398.53	10	209	4618
	Thermal Oil Fluid	Therminol	Toluene	46,467	184	8,568,515	856,851	231,350
			2680	144	386,282.14	10,748.90	10,430	407,461
Acetone	ITC1	Copper	1400	1579	2,321,002.70	0	110,524	2,431,527
	ITC2	Copper	1400	312	458,241.95	1	21,821	480,064
	ITC3	Copper	1400	115	169,131.42	2	8054	177,187
	RHR	Copper	1400	3137	4,611,495.84	3	219,595	4831094
	HTR	Copper	1400	279	409,759.56	4	19,512	429,276
	T1	Copper	1400	2398	3,525,711.97	5	167,891	3,693,608
	T2	Copper	1400	3399	4,996,098.50	6	237,909	5,234,014
	T3	Copper	1400	921	1,353,793.03	7	64,466	1,418,266
	C1	Copper	1400	2822	4,148,525.01	8	197,549	4,346,082
	P1	Copper	1400	2	2889.66	9	138	3036
	P2	Copper	1400	18	26,239.27	10	1249	27,499
	Thermal Oil Fluid	Therminol	Acetone	46,467	184	8,568,515	856,851	231,350
			5426	170	924,019.85	92,401.98	24,949	1,041,370

References

- Diaz, G.A.; Forero, J.D.; Garcia, J.; Rincon, A.; Fontalvo, A.; Bula, A.; Padilla, R.V. Maximum power from fluid flow by applying the first and second laws of thermodynamics. *J. Energy Resour. Technol.* **2017**, *139*, 032903. [\[CrossRef\]](#)
- Ramírez, R.; Gutiérrez, A.S.; Eras, J.J.C.; Valencia, K.; Hernández, B.; Forero, J.D. Evaluation of the energy recovery potential of thermoelectric generators in diesel engines. *J. Clean. Prod.* **2019**, *241*, 118412. [\[CrossRef\]](#)
- Angelino, G. Carbon Dioxide Condensation Cycles. *J. Eneg. Power* **1968**, 287–295. [\[CrossRef\]](#)
- Dostal, V.; Driscoll, M.J.; Hejzlar, P.A. Supercritical Carbon Dioxide Cycle for Next Generation Nuclear Reactors. Ph.D. Thesis, Massachusetts Institute of Technology, Cambridge, UK, March 2004.
- Abrosimov, K.A.; Baccioli, A.; Bisch, A. Techno-economic analysis of combined inverted Brayton—Organic Rankine cycle for high-temperature waste heat recovery. *Energy Convers. Manag.* **2019**, *3*, 100014. [\[CrossRef\]](#)

6. Guo, Z.; Zhao, Y.; Zhu, Y.; Niu, F.; Lu, D. Optimal design of supercritical CO₂ power cycle for next generation nuclear power conversion systems. *Prog. Nucl. Energy* **2018**, *108*, 111–121. [[CrossRef](#)]
7. Padilla, R.V.; Soo Too, Y.C.; Benito, R.; Stein, W. Exergetic analysis of supercritical CO₂ Brayton cycles integrated with solar central receivers. *Appl. Energy* **2015**, *148*, 348–365. [[CrossRef](#)]
8. Padilla, R.V.; Benito, R.G.; Stein, W. An Exergy Analysis of Recompression Supercritical CO₂ Cycles with and without Reheating. *Energy Procedia* **2015**, *69*, 1181–1191. [[CrossRef](#)]
9. Glatzmaier, G.C.; Turchi, C.S. Supercritical CO₂ as a Heat Transfer and Power Cycle Fluid for CSP Systems. In Proceedings of the ASME 2009 3rd International Conference on Energy Sustainability collocated with the Heat Transfer and InterPACK09 Conferences, San Francisco, CA, USA, 19–23 July 2009; pp. 673–676.
10. Hinze, J.F.; Nellis, G.F.; Anderson, M.H. Cost comparison of printed circuit heat exchanger to low cost periodic flow regenerator for use as recuperator in a s-CO₂ Brayton cycle. *Appl. Energy* **2017**, *208*, 1150–1161. [[CrossRef](#)]
11. Sharan, P.; Neises, T.; Turchi, C. Thermal desalination via supercritical CO₂ Brayton cycle: Optimal system design and techno-economic analysis without reduction in cycle efficiency. *Appl. Ther. Eng.* **2019**, *152*, 499–514. [[CrossRef](#)]
12. Park, J.H.; Park, H.S.; Kwon, J.G.; Kim, T.H.; Kim, M.H. Optimization and thermodynamic analysis of supercritical CO₂ Brayton recompression cycle for various small modular reactors. *Energy* **2018**, *160*, 520–535. [[CrossRef](#)]
13. Li, H.; Zhang, Y.; Zhang, L.; Yao, M.; Kruiuzenga, A.; Anderson, M. PDF-based modeling on the turbulent convection heat transfer of supercritical CO₂ in the printed circuit heat exchangers for the supercritical CO₂ Brayton cycle. *Int. J. Heat Mass Transf.* **2016**, *98*, 204–218. [[CrossRef](#)]
14. Ahn, Y.; Bae, S.J.; Kim, M.; Cho, S.K.; Baik, S.; Lee, J.I.; Cha, J.E. Review of supercritical CO₂ power cycle technology and current status of research and development. *Nucl. Eng. Technol.* **2015**, *47*, 647–661. [[CrossRef](#)]
15. Musgrove, G.; Sullivan, S.; Shiferaw, D.; Fourspring, P. Heat exchangers. In *Fundamentals and Applications of Supercritical Carbon Dioxide (SCO₂) Based Power Cycles*; Elsevier Ltd.: Amsterdam, The Netherlands, 2017; pp. 217–244.
16. Jiang, Y.; Liese, E.; Zitney, S.E.; Bhattacharyya, D. Optimal design of microtube recuperators for an indirect supercritical carbon dioxide recompression closed Brayton cycle. *Appl. Energy* **2018**, *216*, 634–648. [[CrossRef](#)]
17. Jiang, Y.; Liese, E.; Zitney, S.E.; Bhattacharyya, D. Design and dynamic modeling of printed circuit heat exchangers for supercritical carbon dioxide Brayton power cycles. *Appl. Energy* **2018**, *231*, 1019–1032. [[CrossRef](#)]
18. Chen, J.; Liu, Y.; Lu, X.; Ji, X.; Wang, C. Designing heat exchanger for enhancing heat transfer of slurries in biogas plants. *Energy Procedia* **2019**, *158*, 1288–1293. [[CrossRef](#)]
19. Pidaparti, S.R.; Anderson, M.H.; Ranjan, D. Experimental Investigation of thermal-hydraulic performance of discontinuous fin printed circuit heat exchangers for Supercritical CO₂ power cycles. *Exp. Ther. Fluid Sci.* **2019**, *106*, 119–129. [[CrossRef](#)]
20. Colonna, P.; van Putten, H. Dynamic modeling of steam power cycles. Part I—Modeling paradigm and validation. *Appl. Ther. Eng.* **2007**, *27*, 467–480. [[CrossRef](#)]
21. Van Putten, H.; Colonna, P. Dynamic modeling of steam power cycles: Part II—Simulation of a small simple Rankine cycle system. *Appl. Ther. Eng.* **2007**, *27*, 2566–2582. [[CrossRef](#)]
22. Chien, N.B.; Jong-Taek, O.; Asano, H.; Tomiyama, Y. Investigation of experiment and simulation of a plate heat exchanger. *Energy Procedia* **2019**, *158*, 5635–5640. [[CrossRef](#)]
23. Liu, Y.; Wang, Y.; Huang, D. Supercritical CO₂ Brayton cycle: A state-of-the-art review. *Energy* **2019**, *189*, 115900. [[CrossRef](#)]
24. Mohammadkhani, F.; Shokati, N.; Mahmoudi, S.M.S.; Yari, M.; Rosen, M.A. Exergoeconomic assessment and parametric study of a Gas Turbine-Modular Helium Reactor combined with two Organic Rankine Cycles. *Energy* **2014**, *65*, 533–543. [[CrossRef](#)]
25. Turchi, C.S.; Ma, Z.; Neises, T.; Wagner, M. Thermodynamic Study of Advanced Supercritical Carbon Dioxide Power Cycles for High Performance Concentrating Solar Power Systems. In Proceedings of the ASME 2012 6th International Conference on Energy Sustainability Collocated with the ASME 2012 10th International Conference on Fuel Cell Science, Engineering and Technology, San Diego, CA, USA, 23–26 July 2012; pp. 375–383.

26. Le Moullec, Y. Conceptual study of a high efficiency coal-fired power plant with CO₂ capture using a supercritical CO₂ Brayton cycle. *Energy* **2013**, *49*, 32–46. [[CrossRef](#)]
27. Olumayegun, O.; Wang, M.; Oko, E. Thermodynamic performance evaluation of supercritical CO₂ closed Brayton cycles for coal-fired power generation with solvent-based CO₂ capture. *Energy* **2019**, *166*, 1074–1088. [[CrossRef](#)]
28. Liang, Y.; Bian, X.; Qian, W.; Pan, M.; Ban, Z.; Yu, Z. Theoretical analysis of a regenerative supercritical carbon dioxide Brayton cycle/organic Rankine cycle dual loop for waste heat recovery of a diesel/natural gas dual-fuel engine. *Energy Convers. Manag.* **2019**, *197*, 111845. [[CrossRef](#)]
29. Kao, S.; Gibbs, J.; Hejzlar, P. Dynamic Simulation and Control of a Supercritical CO₂ Power Conversion System for Small Light Water Reactor Applications. In Proceedings of the Supercritical CO₂ Power Cycle Symposium, Troy, NY, USA, 29–30 April 2009.
30. Uusitalo, A.; Ameli, A.; Turunen-Saaresti, T. Thermodynamic and turbomachinery design analysis of supercritical Brayton cycles for exhaust gas heat recovery. *Energy* **2019**, *167*, 60–79. [[CrossRef](#)]
31. Danieli, P.; Rech, S.; Lazzaretto, A. Supercritical CO₂ and air Brayton-Joule versus ORC systems for heat recovery from glass furnaces: Performance and economic evaluation. *Energy* **2019**, *168*, 295–309. [[CrossRef](#)]
32. Thakar, R.; Bhosle, S.; Lahane, S. Design of Heat Exchanger for Waste Heat Recovery from Exhaust Gas of Diesel Engine. *Procedia Manuf.* **2018**, *20*, 372–376. [[CrossRef](#)]
33. Valencia, G.; Isaza-Roldan, C.; Forero, J. Economic and Exergo-Advance Analysis of a Waste Heat Recovery System based on Regenerative Organic Rankine Cycle under Organic Fluids with Low Global Warming Potential. *Energies* **2020**, *13*, 1317.
34. Ochoa, G.V.; Peñaloza, C.A.; Forero, J.D. Thermo-economic assessment of a gas microturbine-absorption chiller trigeneration system under different compressor inlet air temperatures. *Energies* **2019**, *12*, 4643. [[CrossRef](#)]
35. Valencia, G.; Peñaloza, C.; Rojas, J. Thermo-economic Modelling and Parametric Study of a Simple ORC for the Recovery of Waste Heat in a 2 MW Gas Engine under Different Working Fluids. *Appl. Sci.* **2019**, *9*, 4017. [[CrossRef](#)]
36. Ochoa, G.V.; Isaza-Roldan, C.; Forero, J.D. A phenomenological base semi-physical thermodynamic model for the cylinder and exhaust manifold of a natural gas 2-megawatt four-stroke internal combustion engine. *Heliyon* **2019**, *5*, e02700. [[CrossRef](#)] [[PubMed](#)]
37. Fan, W.; Han, Z.; Li, P.; Jia, Y. Analysis of the thermodynamic performance of the organic Rankine cycle (ORC) based on the characteristic parameters of the working fluid and criterion for working fluid selection. *Energy Convers. Manag.* **2020**, *211*, 112746. [[CrossRef](#)]
38. Iso, T.; Standards, I. *Environmental Management The ISO 14000 Family of International Standards ISO in Brief ISO and the Environment*; International Organization for Standardization: Geneva, Switzerland, 2009.
39. Valencia Ochoa, G.; Cárdenas Gutierrez, J.; Duarte Forero, J. Exergy, Economic, and Life-Cycle Assessment of ORC System for Waste Heat Recovery in a Natural Gas Internal Combustion Engine. *Resource* **2020**, *9*, 2. [[CrossRef](#)]
40. Michos, C.N.; Lion, S.; Vlaskos, I.; Taccani, R. Analysis of the backpressure effect of an Organic Rankine Cycle (ORC) evaporator on the exhaust line of a turbocharged heavy duty diesel power generator for marine applications. *Energy Convers. Manag.* **2017**, *132*, 347–360. [[CrossRef](#)]
41. ASHRAE. *ANSI/ASHRAE Standard 62.1-2010. Ventilation for Acceptable Indoor Air Quality*, 62nd ed.; American Society of Heating, Refrigerating, and Air-Conditioning Engineers, Inc.: Atlanta, GA, USA, 2010.
42. Ke, H.; Xiao, Q.; Cao, Y.; Ma, T.; Lin, Y.; Zeng, M.; Wang, Q. Simulation of the printed circuit heat exchanger for S-CO₂ by segmented methods. *Energy Procedia* **2017**, *142*, 4098–4103. [[CrossRef](#)]
43. Ding, Y.; Liu, C.; Zhang, C.; Xu, X.; Li, Q.; Mao, L. Exergoenvironmental model of Organic Rankine Cycle system including the manufacture and leakage of working fluid. *Energy* **2018**, *145*, 52–64. [[CrossRef](#)]
44. Valencia Ochoa, G.; Piero Rojas, J.; Duarte Forero, J. Advance Exergo-Economic Analysis of a Waste Heat Recovery System Using ORC for a Bottoming Natural Gas Engine. *Energies* **2020**, *13*, 267. [[CrossRef](#)]
45. Valencia, G.; Duarte, J.; Isaza-Roldan, C. Thermo-economic Analysis of Different Exhaust Waste-Heat Recovery Systems for Natural Gas Engine Based on ORC. *Appl. Sci.* **2019**, *9*, 4017. [[CrossRef](#)]
46. Valencia Ochoa, G.; Acevedo Peñaloza, C.; Duarte Forero, J. Thermo-economic optimization with PSO Algorithm of waste heat recovery systems based on Organic Rankine Cycle system for a natural gas engine. *Energies* **2019**, *12*, 4165. [[CrossRef](#)]

47. Preißinger, M.; Brüggemann, D. Thermo-economic Evaluation of Modular Organic Rankine Cycles for Waste Heat Recovery over a Broad Range of Heat Source Temperatures and Capacities. *Energies* **2017**, *10*, 269. [[CrossRef](#)]
48. Tchanche, B.; Lambrinos, G.; Frangoudakis, A.; Papadakis, G. Low-grade heat conversion into power using organic Rankine cycles-A review of various applications. *Renew. Sustain. Energy Rev.* **2011**, *15*, 3963–3979. [[CrossRef](#)]



© 2020 by the authors. Licensee MDPI, Basel, Switzerland. This article is an open access article distributed under the terms and conditions of the Creative Commons Attribution (CC BY) license (<http://creativecommons.org/licenses/by/4.0/>).